Dislocation nucleation from interacting surface corners in silicon

Z. Li and R. C. Picu[a)]
Department of Mechanical, Aerospace and Nuclear Engineering, Rensselaer Polytechnic Institute, Troy, New York 12180, USA

(Received 14 April 2010; accepted 1 July 2010; published online 9 August 2010)

The nucleation of dislocations from sharp corners acting as stress concentration sites on a silicon (100) surface is studied by a combination of atomistic and continuum modeling. Ledges of various heights, similar to those found in microelectronic devices, are considered. In this work we focus on the effect of ledge height and of ledge-ledge elastic interaction on the activation energy for dislocation nucleation. The activation energy decreases slightly with increasing the height of the ledge and has a more pronounced, nonmonotonic variation with the distance between stress concentration sites. The effect of introducing a radius of curvature at the root of the ledge is also studied. It is concluded that even a small radius of curvature renders the nucleation process similar to that from a flat surface of same crystallographic orientation. © *2010 American Institute of Physics*. [doi:10.1063/1.3471801]

I. INTRODUCTION

Dislocation nucleation in microelectronic devices is detrimental as these crystal defects lead to charge leakage and shorts. Therefore, their nucleation was studied extensively over the last decades. Nucleation may take place at 0 K (the athermal limit) under relatively high stresses. In situations of practical importance both thermal fluctuations and stress contribute to overcoming the energy barrier associated with the formation of a new dislocation.

Stress is produced by strained layers, which are used to control the electronic properties of the semiconductor. Residual stresses introduced during processing and/or due to differences in thermal expansion coefficients of constituent materials, or due to implantation, may also be important. The analysis of dislocation nucleation in a strained layer of constant thickness deposited on an unloaded substrate led to the introduction of the concept of "critical thickness" of the strained film, which separates defect-free (thin) and defective (thick) films.[1,2] When the strained layer is discontinuous, the stress field is nonuniform and the analysis of defect nucleation becomes more involved. The corner formed by the edge of the strained film with the substrate is a stress concentration site with large stress/strain gradients. In the so-called "force model" of this problem, the details of the local geometry are ignored and the action of the film on the substrate is represented by a force.[3] More detailed models have been developed based on analytical considerations[4,5] and finite element simulations.[6–9] These, along with the experimental evaluation of the strain fields in such structures have been reviewed by Jain *et al.*[10] More recently, Zhang *et al.*[11] performed an elasticity analysis of the stress concentration at such corners based on the classical formulation due to Williams[12] and Bogy and Wang,[13] deriving the asymptotic field and the associated stress intensity factor, as well as its dependence on the aspect ratio of the strained layer.

Evidence of dislocation nucleation taking place predominantly at surface imperfections such as steps and ledges is ample. For example, Kammler *et al.*[14] observed dislocations being emitted from the corners of SiN pads on Si, provided the size of the pads is large enough (i.e., that sufficient strain energy is stored in the initial strain field). They also observe that the resulting dislocation structure does not depend on the geometric details of the nucleation site but the critical load at which nucleation happens is sensitive to these factors. The dislocation structure below the concentrator could be modeled accurately using dislocation dynamics,[15] which does not incorporate any information on nucleation (a supercritical dislocation loop has to be inserted in the model which, in turn, accounts only for its subsequent evolution). Direct, real time observations of dislocation nucleation in epitaxial Ge islands growing on Si have been performed by LeGoues *et al.*[16] and the process was modeled analytically by Johnson and Freund.[17] The stress concentration at surface steps and ledges leads to preferential dislocation nucleation under other loading conditions as well. For example, during nanoindentation in an otherwise unloaded surface, pop-in events are observed at a smaller applied force in presence of surface steps than in a nominally atomically flat surface.[18]

Dislocation nucleation is a stochastic process which depends on the applied stress (and strain gradients, if nucleation is not homogeneous) and temperature, and is well described by the theory of thermally activated processes. The characteristic parameters are the activation energy and the activation volume, where the second quantity is the derivative of the activation energy with respect to the applied stress. Nucleation is an atomistic process and is best represented by discrete, atomistic models.[19–24] Athermal (0 K) atomistic models are best suited to identify the critical stress at which the process takes place in absence of thermal fluctuations but are limited in their ability to properly define the saddle point configuration and the associated activation energy in situations in which the activation volume is large. On the other hand, finite temperature atomistic models rely on monitoring the dynamics until a nucleation event is observed.[19,20] From this, and using an Arrhenius function for

[a)]Electronic mail: picuc@rpi.edu.

the rate of occurrence, the activation energy can be inferred. However, the observation of an infrequent event requires applying stresses close to the athermal limit and is inherently affected by poor statistics. Due to these issues, it has been common practice to determine the critical configuration using continuum elastic dislocation theory.[25–27] These analyses are more elegant since they allow identifying the essential parameters of the problem and, in some cases, lead to the solution in close form. However, a number of assumptions have to be made: dislocation cores are considered compact and the core structure does not change under stress, a simple shape has to be assumed for the nucleating dislocation, image forces are evaluated in a simplified way, etc.[28] It appears that an approach in which atomistic information is used together with elasticity considerations is optimal.

In this work, the problem of dislocation nucleation from surface imperfections such as ledges and surface steps is considered. The focus is on the effect of the ledge height and of ledge-ledge elastic interaction on the nucleation process, issues that did not receive significant attention so far. This provides information on the ledge separation below which the interaction has to be taken into account when designing against dislocation nucleation in thin film devices. A method combining the advantages of continuum and atomistic simulations is developed and used for this purpose. The article is organized as follows: the model and the methodology used to compute the activation energy are presented in Sec. II, the results are presented and discussed in Sec. III and conclusions are reviewed in closure.

II. MODEL AND METHODS

Dislocations in diamond cubic Si are located either in the glide or in the shuffle set of {111} planes. It has been shown that at low temperatures dislocations with a compact core nucleate in the shuffle plane, while at elevated temperatures dissociated glide dislocations form.[20] Since electronic devices generally function at low Si homologous temperatures, the relevant type of dislocation to be studied is the shuffle one. Figure 1 shows the relative displacement across the glide plane for a 60° shuffle core in Si modeled using the Stillinger–Weber potential. Both axes are normalized with the Burgers vector length, $b=|\mathbf{b}|$. The inset shows a detail of the curve in the main figure. The core is compact both in the bulk and when located close to a free surface. However, in this second case, the core is shifted closer to the surface due to the action of image stresses. The compact core provides significant advantages when investigating the nucleation problem, as discussed below.

Let us consider the configuration in Fig. 2(a). An isolated ledge is defined on the (100) surface of a Si slab, with the height h being an adjustable parameter. The ledge is oriented in the $[01\bar{1}]$ direction such that it is located at the convergence of two glide planes, denoted as GP1 and GP2 in Fig. 2. The corner is considered atomically sharp (as in Refs. 19, 20, and 29). Since this detail is important in nucleation, the effect of the corner curvature is discussed separately. The upper surface is free, the bottom face is prevented from moving in the x_1 direction and periodic boundary conditions are

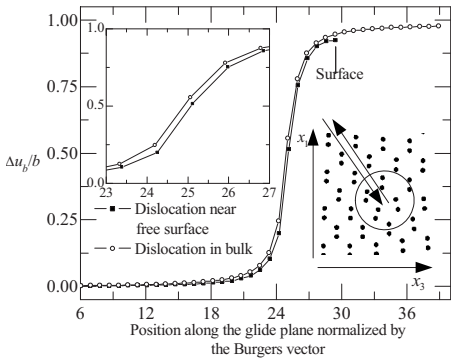

FIG. 1. Core structure (normalized relative displacement in the Burgers vector direction across the glide plane) for shuffle 60° dislocations located in the bulk and close to the free surface. The dislocation resides on glide plane GP1 in Fig. 2(a). The normalization factor is the Burgers vector length, b. The inset shows a detail of the main figure emphasizing the shift in the core located below the free surface under the action of the image stress. The atomistic core structure of the 60° shuffle dislocation in bulk is also shown; the arrows indicate the direction of motion in the glide plane GP1 [Fig. 2(a)] and the circle marks the approximate core center position.

applied in the x_2 direction. These periodic boundary conditions require that the nucleating dislocation is straight. This is a limitation of the present analysis since it is known that dislocations nucleate from surfaces or from ledge edges as half loops. However, since our primary objective is to investigate the effect of the interaction of stress concentration sites on the nucleation process, we choose to consider this configuration which provides significant algorithmic advantages. The overall barrier is expected to decrease if three-dimensional configurations in which dislocations nucleate as loops are considered.

Normal strain is applied in the x_3 direction via displacement-imposed boundary conditions. This produces a stress σ_{33}, while the periodic boundary conditions impose a

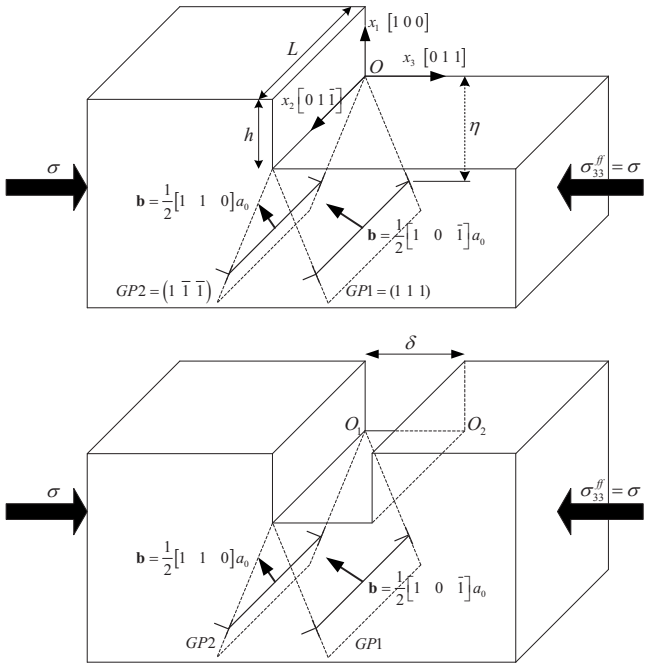

FIG. 2. Schematic representation of models (single and double ledge) used in this work.

nonzero stress σ_{22} (which has no effect on nucleation). The far-field σ_{11} is zero and all far-field shear stress components vanish as well due to the symmetry of the crystal orientation relative to the given coordinate system and far-field loading. This loading is representative for stresses in electronic devices due to thermal and elastic mismatch, implantation and other causes. The dimensions of the model are $42\times23\times90$ nm^3; the model contains approximately half a million atoms. The Stillinger–Weber three-body potential, which has been used extensively in atomistic simulations of Si mechanics, is used to describe the interatomic interactions.[30]

Dislocations nucleating in the two glide planes GP1 and GP2 may be either of 60° or pure screw type. The Taylor factor for the 60° dislocations is $1/\sqrt{6}$ and vanishes for the screw dislocations. Hence, only 60° dislocations may nucleate in this configuration. Out of the four possible orientations of the Burgers vector (in each plane), only those shown in Fig. 2 need to be considered since the nucleation of these dislocations decreases the height of the ledge, therefore, reducing the total surface energy of the model. Obviously, the nucleation barrier for dislocations that decrease the ledge height is smaller than that for dislocations that increase the height or produce steps on the surface, and therefore their nucleation probability is larger. When a compressive far-field σ_{33} is applied, the 60° dislocation in GP1 should be considered, since that in GP2 is expelled from the crystal by the far-field. The situation is opposite when a tensile far-field is applied, case in which nucleation in plane GP2 has to be considered.

Figure 2(b) shows a similar configuration in which two ledges separated by a distance δ are introduced. δ is kept as a parameter which controls the elastic interaction of the two stress concentrators (ledge roots). The coordinate η is the distance from corner O to the current position of the dislocation core, measured in the negative x_1 direction.

A dislocation nucleating from the ledge in GP1 or GP2 is subjected to a driving stress per unit length due to the far-field (which is concentrated at the corner), an image stress due to the presence of the free surface, and a Peierls-type stress induced by the local potential. The total energy (relative to the system without the dislocation) can be written as:

$$E(\eta) = E_0 + E_P + W_{im}(\eta) - W_{ff}(\eta) \tag{1}$$

where E_0 is the energy of the dislocation located at the closest stable position to the corner (let us denote this distance measured in the $-x_1$ direction by ξ), while W_{im} and W_{ff} are the work done by the image and far-field forces, respectively. The work (per unit length of dislocation line) is evaluated as

$$W_{im} = \int_{\xi}^{\eta} \sigma_{ij}^{im} b_i n_j \frac{dx_1}{n_3},$$

$$W_{ff} = \int_{\xi}^{\eta} \sigma_{ij}^{ff} b_i n_j \frac{dx_1}{n_3}, \tag{2}$$

where $\boldsymbol{\sigma}^{im}$ and $\boldsymbol{\sigma}^{ff}$ are the stress at the current location of the dislocation (defined by the coordinate x_1) produced by the interaction with images and by the far-field, respectively, and $\mathbf{n}$ is the normal to the glide plane.

When too close to the surface, the core is unstable due to the large image force which tends to remove the dislocation from the crystal. In absence of the Peierls potential, there is only one equilibrium configuration for given far-field, configuration defined by the balance of the far-field and image forces. However, since the Peierls potential for the compact core of Fig. 1 is relatively deep, a large number of such minima result. ξ denotes the distance from O to the first such trapped position. At ξ, the dislocation is marginally stable and the core is somewhat distorted; the shape of this core is shown in Fig. 1. As can be seen from the inset, the image force pulls the core in the direction of the free surface (to the right in this figure) by about $1/4b$ from the minimum of the trapping potential well (where the bulk dislocation core resides). E_0 is computed as the energy difference between the model with the dislocation at ξ and the original model without the dislocation, and includes the contribution of W_{im} and W_{ff}. In principle, the integral would give a slightly larger value than obtained by the present method because the dislocation at ξ is trapped in the Peierls valley. However, since ξ is the first equilibrium position close to the surface, the trapping is marginal.

The image stress $\boldsymbol{\sigma}^{im}$ is computed using the superposition method commonly employed in dislocation dynamics simulations to account for image effects:[31] the stress at sites along the half planes defined by $x_1=0$, $x_3>0$, and $x_1=h$, $x_3<0$, produced by the dislocation located in an infinite crystal at position η is computed. The actual model without the dislocation is then considered and the negative of the tractions corresponding to these stress values are applied on the surface. A finite element model is used to evaluate the stress state $\boldsymbol{\sigma}^{im}$ at η, i.e., where the dislocation is to be positioned.

The Peierls barrier E_P is computed by considering an unloaded bulk crystal, using the climbing image nudged elastic band (NEB) method.[32] The core is relaxed in two neighboring Peierls valleys and 13 replicas are constructed interpolating linearly between these two configurations. The NEB procedure is then used to compute the saddle point energy. For this compact shuffle core, the barrier is 0.033 65 eV/Å. It is noted that the motion of real dislocations with compact cores at low temperature involves the formation of kinks. This is not considered here as we assume that the dislocation line remains straight at all times. As discussed above, this is expected to affect slightly the values of the energies involved but should leave unchanged the conclusions related to the effect of the ledge interaction on nucleation.

The accuracy of the Peierls barrier depends on the ability of the potential employed to capture large lattice distortions. As well-known, empirical potentials have significant limitations in this respect. For example, a higher barrier results if the Tersoff potential is used. However, it is generally considered that the Stillinger–Weber potential used in this work is more adequate for representing large lattice deformations than the Tersoff potential.

It should be observed that using the procedure described above, which makes use of atomistic and continuum models, is facilitated by the compact core of the shuffle dislocation (Fig. 1). An extended core would require more extensive use of atomistic models.

III. RESULTS AND DISCUSSION

The stress state close to point O (Fig. 2) is described by the series:

$$\sigma_{ij}^{ff} = \sum_m K_m r^{-\lambda_m} f_{ij}^{(m)}(\theta), \tag{3}$$

where r and θ are radial and angular coordinates in a polar coordinate system centered at O and contained in the x_1-x_3 plane. r represents the distance to the corner. The exponents λ and the angular functions f result from the solution of an eigenvalue problem and the sum in (3) is over the entire set of eigenvalues/eigenvectors. In the limit $r \to 0$, the singular terms in (3), $\lambda_m > 0$, dominate (the asymptotic solution). For the type of concentrator considered here, the solution was obtained by Williams.[12] Two eigenvalues lead to stress concentration: $\lambda_1 = 0.455$ and $\lambda_2 = 0.09$ (values for the isotropic case). These correspond to symmetric and antisymmetric eigenfunctions f, respectively. Since the applied field does not have any particular symmetry relative to the ledge corner, both singular terms are present in (3). A similar analysis was performed by Zhang *et al.*[11] who studied the case in which loading is provided by a residual stress in the ledge (taken as a segment of a strained film).

The quantity of interest in the problem considered here is the normalized resolved shear stress in the Burgers vector direction due to the far-field as follows: $\tau^{*ff} = \sigma_{ij}^{ff} b_i n_j / \sigma b$, where the normalization is made with the $\sigma_{33} = \sigma$ component of the far-field (Fig. 2). Note that the force per unit length of dislocation line acting perpendicular to the dislocation and driving it into the crystal is given by $\tau^{*ff} \sigma b = \sigma_{ij}^{ff} b_i n_j$.

Figure 3(a) shows τ^{*ff} as a function of the distance from O. Far from the corner, τ^{*ff} converges to the Taylor factor $1/\sqrt{6}$, while close to the corner it is singular. The leading term in Eq. (3) varies as $\tau^{*ff} \sim r^{-\lambda_1}$. The two curves in Fig. 3(a) are obtained from a purely atomistic model and from a linear elastic finite element model using elastic constants matching those of the atomistic model. The atomistic stress is evaluated with the virial formula. The results agree well, except in the first two atomic layers at the surface. This observation is important. It implies that in order to evaluate the work terms in Eq. (1) one does not need to develop an atomistic model; the fields resulting from a continuum elastic model are sufficient. The error observed at the surface is not important since Eq. (1) is used for $x_1 > \xi$ and $\xi > 2a_0$ in all cases, where a_0 is the lattice parameter of Si (5.43 Å).

A similar conclusion is obtained for the image term. Figure 3(b) shows the normalized resolved shear stress in the Burgers vector direction produced by the image effect: $\tau^{*im} = \sigma_{ij}^{im} b_i n_j / \sigma b$. While the stress distribution in Fig. 3(a) is produced by the far-field and exists with or without the dislocation, the stress in Fig. 3(b) is produced by the interaction of the dislocation with its image and only the value of the stress at the location of the dislocation, η, is relevant. The stress has a $\tau^{*im} \sim 1/r$ singularity (see inset) and decays to zero as $r \to \infty$.[33] The two curves correspond to values computed using the method described in Sec. II (using a finite element model) and with a purely atomistic model.

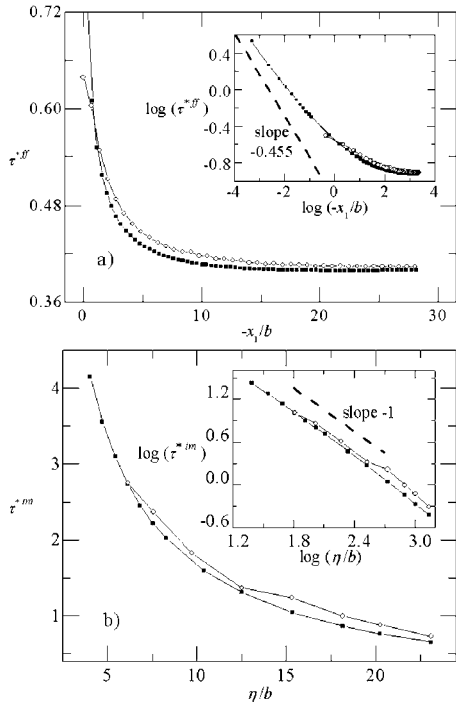

FIG. 3. Variation in the normalized resolved shear stress (a) $\tau^{*ff} = \sigma_{ij}^{ff} b_i n_j / \sigma b$ due to the far-field, and (b) $\tau^{*im} = \sigma_{ij}^{im} b_i n_j / \sigma b$ due to the image effect, with the distance from the ledge corner, O. The open and filled symbols correspond to results obtained from the atomistic and continuum models, respectively. The insets show log-log plots of the quantities in the main figure demonstrating the power law variation of the field in the vicinity of the corner.

To evaluate the image stress from an atomistic model, the dislocation is placed at some position η below the surface, where the Peierls stress stabilizes the core. The model is relaxed under the boundary conditions described in Sec. II, with no applied far-field. The **J** integral is computed along a path Γ encircling the core and contained in the plane x_1-x_3. Let $\hat{\mathbf{n}}$ be the outer normal to this path Γ and $\hat{\mathbf{x}}$ be a two-dimensional rectangular coordinate system centered at O and contained in the plane x_1-x_3. The **J** integral vector $J_k = \int_\Gamma ((1/2)\sigma_{ij}^{im} \varepsilon_{ij}^{im} \hat{n}_k - \sigma_{ij}^{im} \hat{n}_j (\partial u_i / \partial \hat{x}_k)) d\Gamma$ provides the energetic force per unit length of the dislocation due to the image stress. The component of this vector in the glide direction provides the energetic force for glide and equals $\tau^{*im} \sigma b$. Hence, one may compute the **J** integral using the atomistic values for (virial) stress and strain and then evaluate τ^{*im}. This procedure is repeated for various positions η of the core relative to the surface. The results from the continuum and atomistic models shown in Fig. 3(b) are in good agreement.

The variation in the system energy (per unit thickness of the model, E/L) with the position of the dislocation is computed using the procedure outlined in Sec. II. An example for the case with $h/b = 4.24$ and applied far-field strain $\varepsilon_{33}^{ff} = -0.5\%$ ($\sigma_{33} = \sigma = -657$ MPa) is shown in the inset to Fig. 4. The activation energy for nucleation, E_a, is given by the highest point on this curve (1.12 eV/Å). The main figure shows the variation in E_a with the far-field strain. As expected, the activation energy depends strongly on the far-field loading. The curve can be fitted with the equation $E_a/L = C[1 - (\varepsilon_{33}^{ff}/\tilde{\varepsilon}_{33}^{ff})^p]^q$,[34] where $\tilde{\varepsilon}_{33}^{ff}$ is the athermal nucle-

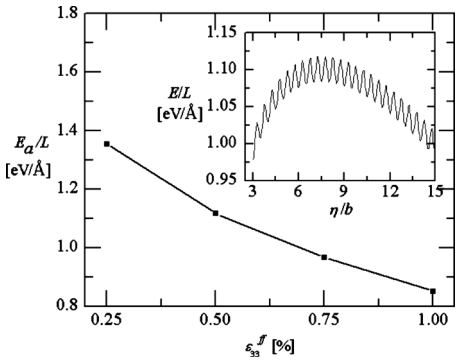

FIG. 4. Variation in the activation energy for nucleation with the far-field applied strain. The inset shows the variation in the energy of the system with the position of the dislocation relative to O, η, for an applied strain $\varepsilon_{33}^{ff}=-0.5\%$.

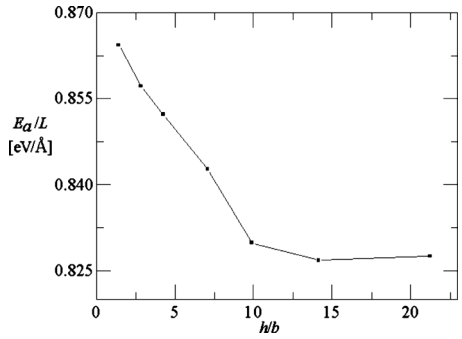

FIG. 5. Variation in the activation energy with the height of the ledge for an applied strain $\varepsilon_{33}^{ff}=-1.0\%$.

ation strain, with $p=0.35$ and $q=1.89$. The value of $\tilde{\varepsilon}_{33}^{ff}$ is approximately 13%, as also obtained at low temperatures by Izumi and Yip[29] and Godet *et al.*[20] for the same type of dislocation.

The data in Fig. 4 provide the activation energy for the configuration with the highest probability of dislocation nucleation (the slip system with the highest resolved shear stress and minimum image force) for the given geometry. To further investigate this issue, glide planes parallel to those shown in Fig. 2 but intersecting the surface at some distance from the ledge corner O were considered. The activation energy for all of these is larger than for the case discussed above (Fig. 4). In the limit, nucleation from a flat surface requires an activation energy of $E_a/L=1.799$ eV/Å, 1.613 eV/Å, and 1.368 eV/Å for far-field strains of $\varepsilon_{33}^{ff}=-0.25\%$, -0.5%, and -1%, respectively. The difference between these values and those reported in Fig. 4 is due primarily to the formation of a surface step when nucleation takes place from the free surface. The energy of the step is included in E_0 of Eq. (1). Nucleation from the corner may lead to either an increase or a decrease in the ledge height, however, only cases in which the height decreases are considered in this analysis as they correspond to smaller activation energies and higher probability of dislocation nucleation.

It is interesting to consider the nucleation from a similar surface feature but in a crystal with a free surface of (111) type. The Peierls barrier remains essentially unchanged but the work done by the far-field and the image stress changes. This is due to the fact that the Taylor factor for the glide plane with the most favorable orientation emerging from the corner decreases, and hence the driving force for nucleation due to the far-field also decreases. Interestingly, the resolved shear stress due to the image effect increases, which again makes nucleation more difficult. Therefore, the geometries discussed in this article are the most favorable for dislocation nucleation among all situations involving (100) and (111) oriented crystals.

Let us discuss now the effect of the ledge height h on the activation energy for dislocation nucleation. Modifying parameter h leads to the variation in both the stress concentration effect [through the variation in the stress intensity factor K_1 in Eq. (3)] and the image contribution. Specifically, as h increases, the image effect decreases, while the concentration effect increases slightly. The effective activation energy per unit length of dislocation line for the case with $\varepsilon_{33}^{ff}=-1\%$ is shown in Fig. 5. The activation energy decreases (and the dislocation nucleation probability increases) as the ledge height increases. The effect is more pronounced at large applied stress.

The effect of ledge-ledge interaction on the nucleation process is discussed next. A model with two ledges is considered [Fig. 2(b)] and the distance between them, δ, is adjusted while keeping $h/b=7$. Two values of the far-field are considered: $\varepsilon_{33}^{ff}=-0.5\%$ and -1%. The activation energy is shown in Figs. 6(a) and 6(b). The values for the isolated ledge ($\delta\to\infty$) are shown as horizontal asymptotes (dashed lines). The activation energy is smaller than the value for an isolated ledge and the convergence to the asymptote is rather slow. This is due to the elastic interaction between ledges which may be characterized by evaluating the stress intensity factor of the most singular term in the asymptotic expansion

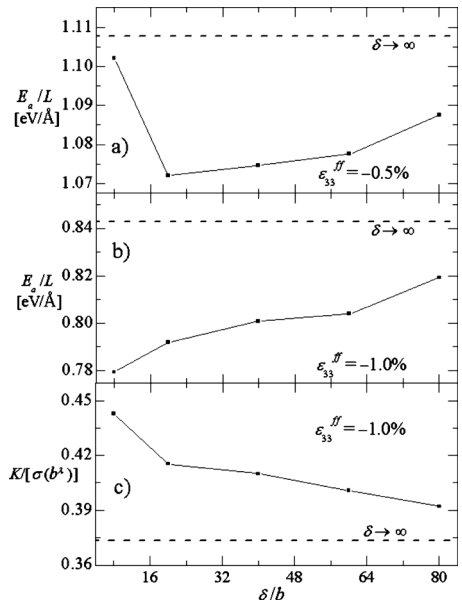

FIG. 6. Variation of the activation energy per unit length of dislocation line with the separation distance between ledges δ/b and for compressive far-fields (a) $\varepsilon_{33}^{ff}=-0.5\%$ and (b) $\varepsilon_{33}^{ff}=-1\%$. The ledge height is $h/b=7$. (c) Variation in the stress intensity factor of the most singular term in Eq. (3) with δ/b. The respective values corresponding to noninteracting ledges ($\delta\to\infty$) are shown with dashed lines.

of Eq. (3) as a function of the relative position of the two ledges. The variation in this parameter with δ at applied far-field $\varepsilon_{33}^{ff}=-1\%$ is shown in Fig. 6(c). A slow convergence to the $\delta\to\infty$ asymptote is observed in this case too.

It should be observed that E_a/L is not monotonic with δ; this is more visible at small ε_{33}^{ff}. The effect is due to the competition between the variation with δ of the energetic force acting on the dislocation produced by the far-field and the image effect. As δ decreases, both the image and far-field contributions increase but their relative importance does not remain constant.

In order to investigate the limit of surface steps (ledge height equal to one atomic plane, $h/b=\sqrt{2}$), we consider the configuration in Fig. 2(b), with $\delta/b=8$. The activation energy results $E_a/L=0.82$ eV/Å at $\varepsilon_{33}^{ff}=-1\%$, i.e., in agreement with the data in Fig. 6(b), after taking into account the correction for the ledge height predicted by the extrapolation of the curve in Fig. 5 (which leads to an estimate of $E_a/L=0.81$). It is interesting to note that if one considers surface steps of "same sign" (as opposed to the configuration in Fig. 2(b), where the surface ledges are of "opposite sign"), the activation energy and its dependence on stress are almost identical. Furthermore, nucleation from the two steps is equally probable.

The activation energy depends strongly on the geometry of the body in which the process takes place and on the geometry of the concentrator. For example, the nucleation of partials from a straight crack front in Cu requires an activation energy of 1.1 eV,[23] while the same dislocation nucleating in a Cu nanopillar of square cross-section requires only 0.016 eV to nucleate,[35] both estimates corresponding to a far-field loading of 75% of the athermal limit. In the present context, the geometry at the root of the ledge is expected to have an important effect on nucleation. For a perfectly sharp corner (Fig. 2) and based on a continuum model, the far-field is singular at the root [Eq. (3)]. A nonvanishing radius of curvature eliminates the singularity but the local stress is still larger than elsewhere in the model.

When the corner is rounded, nucleation leads to the formation of a surface step. Hence, this case is closer to nucleation from a flat surface than to nucleation from a perfectly sharp corner. Clearly, the only difference between nucleation from a flat surface and nucleation from a rounded corner is the stress concentration at the corner. It is useful to determine how fast the rounded corner case converges to the flat surface case as the radius of curvature at the ledge root increases. To investigate this issue we apply to the corner O in Fig. 2 a radius of curvature R/b and compute the stress normal to the plane bisecting the corner (the angle made by x_1 and x_3), Fig. 7. The variation in the stress along axis $\hat{x}_1$ (inset to Fig. 7) is shown for $R/b=0$, 10, and 20. The sharp corner leads to a strong concentration at O, while for $R/b=20$, the concentration effect is largely lost. This indicates that even small radii of curvature render nucleation from the ledge root quite similar to nucleation from the flat surface.

IV. CONCLUSIONS

Dislocation nucleation at surface imperfections such as steps or ledges is favored relative to nucleation from a perfect free surface due to (a) the far-field stress concentration at such locations, and (b) to the fact that the image effect is weakened by the presence of the ledge. In addition, an atomically sharp ledge may decrease in height upon dislocation nucleation from its root, which significantly reduces the activation energy for nucleation. Increasing the ledge height decreases the activation energy slightly, while the elastic interaction of neighboring ledges also decreases the activation energy. Introducing a radius of curvature at the root of the ledge renders nucleation from the respective site rather similar to nucleation from a flat surface.

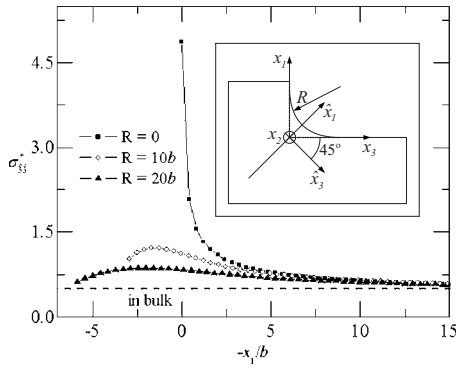

FIG. 7. Variation in the normal stress $\sigma^{\hat{x}}_{\hat{3}\hat{3}}$ (normalized with the far-field, σ) along the bisector $\hat{x}_1$ for a ledge of height $h/b=21.2$ loaded as shows in Fig. 2 and having various radii of curvature R/b at the root. The concentration effect is largely lost as R/b increases. The inset shows the geometry of the corner and the coordinate system used for the evaluation of the stress.

ACKNOWLEDGMENTS

This work was supported by IBM and the Center for Computational Nanotechnology Innovation (CCNI) at Rensselaer Polytechnic Institute.

[1] J. Zou and D. J. H. Cockayne, J. Appl. Phys. **79**, 7632 (1996).
[2] L. B. Freund and S. Suresh, *Thin Film Materials* (Cambridge University Press, New York, 2003).
[3] See, e.g., S. M. Hu, J. Appl. Phys. **70**, R53 (1991).
[4] E. Suhir, ASME J. Appl. Mech. **53**, 657 (1986).
[5] S. Luryi and E. Suhir, Appl. Phys. Lett. **49**, 140 (1986).
[6] S. C. Jain, A. H. Harker, A. Atkinson, and K. Pinardi, J. Appl. Phys. **78**, 1630 (1995).
[7] A. H. Harker, K. Pinardi, A. Atkinson, and S. C. Jain, Philos. Mag. A **71**, 871 (1995).
[8] P. Van Mieghem, S. C. Jain, J. Nijs, and R. Van Overstraeten, J. Appl. Phys. **75**, 666 (1994).
[9] S. Isomae, J. Appl. Phys. **52**, 2782 (1981).
[10] S. C. Jain, H. E. Maes, K. Pinardi, and I. De Wolf, J. Appl. Phys. **79**, 8145 (1996).
[11] Z. Zhang, J. Yoon, and Z. Suo, Appl. Phys. Lett. **89**, 261912 (2006).
[12] M. L. Williams, ASME J. Appl. Mech. **19**, 526 (1952).
[13] D. B. Bogy and K. C. Wang, Int. J. Solids Struct. **7**, 993 (1971).
[14] M. Kammler, D. Chidambarrao, K. W. Schwarz, C. T. Black, and F. M. Ross, Appl. Phys. Lett. **87**, 133116 (2005).
[15] K. W. Schwarz and D. Chidambarrao, J. Appl. Phys. **85**, 7198 (1999).
[16] F. K. LeGoues, M. C. Reuter, J. Tersoff, M. Hammar, and R. M. Tromp, Phys. Rev. Lett. **73**, 300 (1994).
[17] H. T. Johnson and L. B. Freund, J. Appl. Phys. **81**, 6081 (1997).
[18] J. A. Zimmerman, C. L. Kelchner, P. A. Klein, J. C. Hamilton, and S. M. Foiles, Phys. Rev. Lett. **87**, 165507 (2001).
[19] P. Hirel, J. Godet, S. Brochard, L. Pizzagalli, and P. Beauchamp, Phys. Rev. B **78**, 064109 (2008).
[20] J. Godet, P. Hirel, S. Brochard, and L. Pizzagalli, J. Appl. Phys. **105**, 026104 (2009).

[21]J. K. Diao, K. Gall, and M. L. Dunn, Nano Lett. **4**, 1863 (2004).
[22]E. Rabkin, H. S. Nam, and D. J. Srolovitz, Acta Mater. **55**, 2085 (2007).
[23]T. Zhu, J. Li, and S. Yip, Phys. Rev. Lett. **93**, 025503 (2004).
[24]F. Cleri, S. Yip, D. Wolf, and S. R. Phillpot, Phys. Rev. Lett. **79**, 1309 (1997).
[25]S. V. Kamat and J. P. Hirth, J. Appl. Phys. **67**, 6844 (1990).
[26]G. E. Beltz and L. B. Freund, Phys. Status Solidi B **180**, 303 (1993).
[27]G. E. Beltz and L. B. Freund, Philos. Mag. A **69**, 183 (1994).
[28]G. Xu and C. Zhang, J. Mech. Phys. Solids **51**, 1371 (2003).
[29]S. Izumi and S. Yip, J. Appl. Phys. **104**, 033513 (2008).
[30]F. H. Stillinger and T. A. Weber, Phys. Rev. B **31**, 5262 (1985).
[31]H. H. M. Cleveringa, E. van der Giessen, and A. Needleman, Acta Mater. **45**, 3163 (1997).
[32]G. Henkelman, B. P. Uberuaga, and H. Jonsson, J. Chem. Phys. **113**, 9901 (2000).
[33]J. R. Rice, in *Fundamentals of Deformation and Fracture*, edited by B. A. Bilby, K. J. Miller, and J. R. Willis, (Cambridge University, Cambridge, 1984), p. 33.
[34]U. F. Kocks, in *Constitutive Equations in Plasticity*, edited by A. S. Argon (MIT, Cambridge, 1975), p. 81.
[35]T. Zhu, J. Li, A. Samanta, A. Leach, and K. Gall, Phys. Rev. Lett. **100**, 025502 (2008).